Direct Research Journal of Engineering and Information Technology
Vol. 12 (2), Pp. 104-120, July 2024
ISSN: 2354-4155
DOI: https://doi.org/10.26765/DRJEIT4891933670
Article Number: DRJEIT4891933670

https://journals.directresearchpublisher.org/index.php/drjeit

Evaluation of the Corrosion Inhibition Performance of Orange Leaf Extract on Aluminum in Basic Media

Innocent Ugochukwu Okonkwo*, Rowland Ugochukwu Azike and Elohor Diamond Akpobi

Department of Chemical and Petroleum Engineering, College of Engineering, Igbinedion University, Okada, Edo Sate, Nigeria.

Corresponding Author E-mail: innocent.okonkwo@iuokada.edu.ng; https://orcid.org/0009-0007-7855-8775

Received 9 June 2024; Accepted 19 July 2024; Published 26 July 2024

ABSTRACT: The research used gravimetric and electrochemical methods to study the effect of orange leaf extract (OLE) on aluminum corrosion in alkaline conditions. Characterization involved Fourier Transform Infrared Spectroscopy (FTIR) for material analysis, and Electron Dispersive X-ray Spectroscopy (EDX) and Scanning Electron Microscopy (SEM) for surface morphology examination. Results show that OLE effectively inhibits aluminum corrosion under basic conditions, with up to 90% inhibition efficiency at 303 K and 84.85% at 313 K. The inhibition efficiency decreases with higher temperatures and longer immersion times, but increases with higher extract concentrations. OLE is identified as a potential corrosion inhibitor for aluminum in alkaline environments, attributed to the adherence of inhibitor molecules to the aluminum surface, primarily through O-H and N-H functional groups. Additionally, the extract acts as a mixed-type inhibitor, creating a protective coating on the metal surface and showing the hydrophobic nature of aluminum in the presence of the inhibitor. This study highlights the effectiveness of orange leaf extract as a corrosion inhibitor for aluminum in basic media.

Keywords: Aluminum, orange leaf extract, inhibitor, corrosion, gravimetric, electrochemical
Citation Okonkwo,I. U., Azike, R. U., and Akpobi,E. D. (2024). Evaluation of the Corrosion Inhibition Performance of Orange Leaf Extract on Aluminum in Basic Media. Direct Res. J. Eng. Inform. Tech. Vol. 12 (2), Pp. 104-120. https://doi.org/10.26765/DRJEIT4891933670

INTRODUCTION

The depletion of valuable resources such as iron, aluminum, copper, chromium, manganese, and titanium is a pressing concern for nations. The imminent scarcity of these metals is a looming reality that must be addressed. Understanding the destructive impact of corrosion on these essential materials and the potential of corrosion protection technology to mitigate this issue is crucial for conservation efforts. Aluminum, in particular, holds significant economic importance across various industries, yet it is highly susceptible to corrosion in harsh environmental conditions, which may consist of liquids, gases, or mixtures. Corrosion, a natural deterioration process caused by the reaction of materials with their surroundings, is not limited to metals but also affects other substances (Putilora et al., 1960; Fontana and Greener, 1978). Corrosion not only decreases an object's usefulness and lifespan but also poses serious safety and economic repercussions through structural damage (Adegbite et al., 2006). Electrochemical corrosion is the most common type, involving electron transfer across a metal surface, requiring an electrolyte like water or moisture and an electrochemical cell with an anode and a cathode (Yanxia et al., 2022). The process of corrosion in industries, such as oil and natural gas pipelines and industrial plant construction, is primarily driven by the metal oxidation process. This involves the production of metal ions at the anode, while a different species, typically oxygen or hydrogen ions, is reduced at the cathode (Boffarh, 2003; Priya, 2017). Given the importance of this process, protecting metals with inhibitor applications is crucial, particularly in corrosive environments. However, due to restrictions on toxic compounds, there is a growing demand for alternative corrosion inhibitors (Leelavathi and Rajalakshmi, 2013). As a result, there is increasing exploration of natural organic inhibitors derived from plant extracts, which contain phytochemical components. These inhibitors are being considered as safer and eco-friendly options to

form protective layers on metal surfaces, thereby inhibiting the oxidation and reduction phases of the redox reaction (Tan et al., 2021; Frank and Jhon, 1979; Miralrio and Vázquez, 2020).

This study used non-electrochemical methods to assess the inhibitory effects of Citrus sinensis leaf extract on aluminum corrosion. The focus was on the use of the alcoholic component of the extract for corrosion suppression. Aluminum, valued for its strength and endurance, is commonly used in gas cylinders and vehicles for gas transportation but is prone to corrosion. Corrosion can lead to decreased strength, structural decay, loss of product value, and contamination of fluids in pipelines and containers, impacting the reliability of systems in transportation, oil, gas, chemical, and automotive industries (Aiawadhi et al., 2008; Victoria et al., 2015).

The oil and gas, and petrochemical sectors rely heavily on thousands of kilometers of pipelines, pumps, pressure vessels, and storage facilities for the processing, storing, and transportation of various products. These critical infrastructures play an indirect yet essential role in supporting the national economy. However, a significant concern arises from the fact that a majority of these installations and their components are made of aluminum, making them susceptible to corrosion and deterioration over time. The potential consequences of such degradation are far-reaching, including product spills that pose risks to both public safety and the environment, as well as causing substantial financial and time losses in production. Additionally, the involvement of compensation and legal actions further exacerbates the impact, leading to undesirable publicity. As a result, there is a paramount emphasis on the rigorous observation and examination of these establishments to mitigate these risks and ensure operational integrity.

Aluminum, with its exceptional qualities such as easy availability, high strength, and durability, is widely utilized in various industries. It is commonly used in the construction of reaction vessels and tanks to handle corrosive liquids and create aggressive solutions including acidic, basic, and salt solutions. In petrochemical processes, basic solutions play a crucial role in activities such as cleaning, chemical production, and polymer manufacturing. For instance, sodium hydroxide solutions are employed in the extraction of hydrogen sulfide and mercaptans during petroleum refining. Basic solutions are also essential in the production of organic compounds, with epoxypropane being a significant ingredient for the production of polyurethanes. Furthermore, fundamental solutions are extensively used in oil exploration, production, drilling, hydraulic fracturing, and descaling activities. However, it is important to note that aluminum is susceptible to corrosion in basic environments due to interfacial reactions that dissolve the metal and lead to the release of ions. This susceptibility can result in localized perforation of the aluminum oxide film, causing faster attack and corrosion. Notably, aluminum is more prone to attack in alkaline conditions compared to acidic environments, and exposure to extremely strong alkaline environments can lead to severe corrosion such as metal pitting (Izionworu et al., 2020).

The phenomenon of corrosion, as described by Bhardwaj (2017), is a natural electrochemical process driven by the potential difference between acid and metal. Dissolved oxygen and hydrogen ions are recognized as the primary catalysts for corrosion, and understanding the causes of corrosion is crucial for effective management (Izionworu et al., 2020). Various substances, including CO_2, water, and acid-base combinations, have been identified as agents that induce corrosion, particularly in the oil and gas industry. Effective and economical corrosion control methods are essential for optimizing earnings and reducing the costly impact of metal deterioration. Corrosion inhibitors play a vital role in preventing metal corrosion in industries and other fields, offering a cost-effective solution to mitigate the effects of corrosive agents (Utility, 1975). The industrial application of corrosion mitigation solutions is widespread, encompassing various sectors such as crude oil extraction, water treatment, manufacturing processes, and infrastructure maintenance. Understanding the intricate interactions of inhibitor compounds with electrochemical systems is a complex task due to the proprietary nature and diverse compositions of these compounds (Bhardwaj, 2017). Mechanistic characterization through surface analysis and electrochemical tests is essential to evaluate the effectiveness of inhibitor compounds and their interactions with corrosion products. Investigative techniques can provide valuable insights into secondary inhibition mechanisms and synergistic effects, shedding light on the diverse behavior of inhibitors with similar chemical structures.

Figure 1, depicts the orange (*Citrus sinensis*) tree, which is a member of the Rutaceae family. *Citrus sinensis* is also known as sweet orange. The leaves are large, long, and pointed, with a strong, smooth, and uniform texture. They are also shiny and yellowish green in color. The little, heart-shaped leaves on the front of each leaf on lemons and limes set them apart from oranges. Oranges are a hybrid of pomelos (Citrus maxima) and mandarins (Citrus reticulata).

The sweet orange was first mentioned in Chinese literature in 314 BC. The orange originated in a region that included southern China, India, and Africa. In 1987, orange trees were the most popular fruit trees produced worldwide. Orange trees are widely grown in tropical and subtropical areas due to their wonderful fruit. Orange flesh contains 87% water, 12% carbohydrates, 1% protein, and very little fat. Orange flesh is a good source of vitamin C and has 47 calories per 100 grams, or 64% of the Daily Value. No other micronutrients are present in

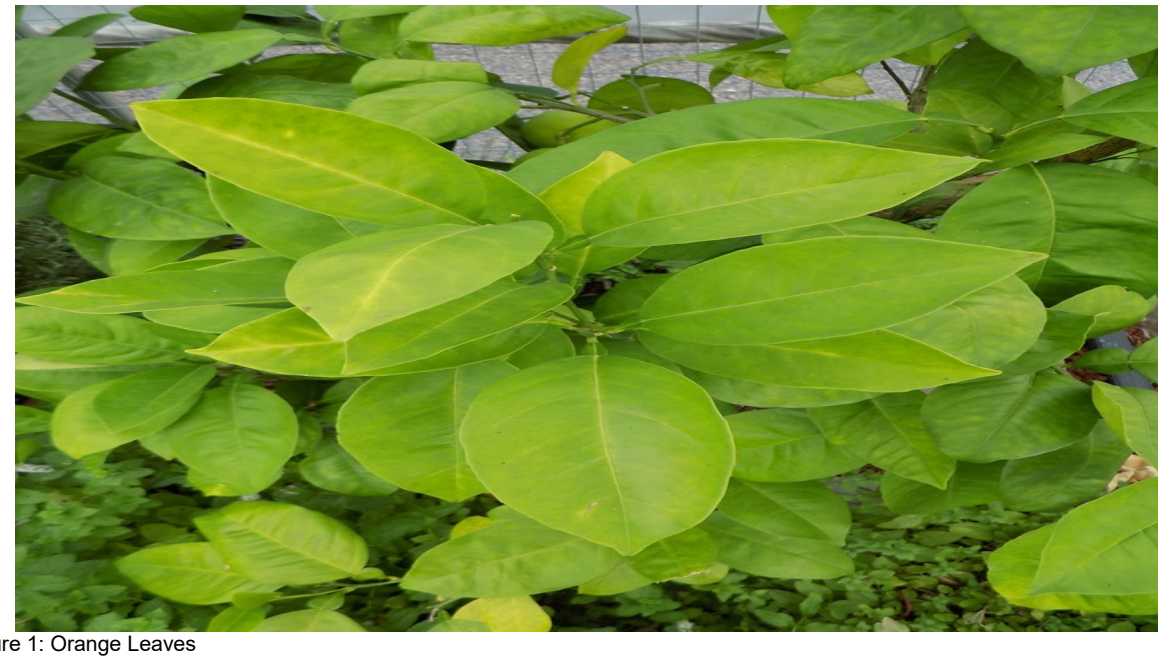

Figure 1: Orange Leaves

concentrations that are meaningful. Numerous volatile organic substances, including as alcohol, aldehydes, and esters, as well as flavonoids and carotenoids (betacarotene, lutetin), are found in orange leaves. The main flavonoid in olive leaf extracts, quercetin, is responsible for the antibacterial action of the extracts while also having antidiarrheal properties. The bioactive and therapeutic activities of OLs are mainly determined by the presence of a distinct variety of bioactive polyphenolic chemicals (e.g., quercetin and other flavonoids) as well as ferulic, caffeine, and gallic acids (Chen and Yen, 2007; Farag et al., 2020).

These phenolic substances are classified as secondary metabolites because of their potent immune-stimulating and antioxidant properties. According to Chen and Yen (2007), orange leaves are also frequently utilized for their anti-inflammatory, anti-diabetic, anti-hypertensive, anti-obesity, anti-spasmodic, cough sedative, and anti-diarrheic qualities. The potential of OL isolates as strong cytotoxic, antitumor, and anticancer drugs has also been demonstrated by research on animal models (Ashraf et al., 2016; Jiang et al., 2020). This study aims to explore the corrosion-inhibiting properties of orange leaf extract on aluminum in basic media.

MATERIALS AND METHODS

Materials collection and preparation

Preparation of aluminium sample

The aluminum was mechanically chopped into 3 × 3 mm coupons in preparation for the gravimetric examination. Using plastic thread, a tiny hole was created at one end of the coupons to enable their suspension in the test solution. The aluminum specimen for the electrochemical investigations was trimmed to a 10 × 10 mm size. Using silicon carbide emery paper of various grades (400 to 1200 grit), the mechanically abraded coupons' surfaces were prepared. They were then cleaned with acetone, rinsed with distilled water, and kept in a desiccator until needed.

.

Base preparation

In order to create a corrosive environment, 28 mL of 98% NaOH (Merck) stock were diluted with distilled water and added to a 1 L standard flask to create a 0.5 M NaOH solution.

Preparation of OLE

Orange leaves were gathered from a garden in Okada, Nigeria's Edo State. The leaves were pounded into a powder after being dried for seven days out of the sun. First, 100 g of the powdered leaf were weighed and incubated for 48 hours in a 500 mL beaker of ethanol. The extract was filtered through Whatman filter paper (grade 1) after it was evaporated using a rotary evaporator. Three different concentrations of 0.3, 0.6, and 0.9 g/L were used to prepare the extract.

Examining the extracts phytochemically

The extracts were screened phytochemically using reagents including Meyer's, aqueous NaOH, acetic anhydride, 1% $FeCl_3$, and copper sulphate solution to find

secondary metabolites such alkaloids, flavonoids, tannins, saponin, and protein.

Flavonoids determination

At room temperature, 100ml of 80% aqueous methanol was used to extract 5g of the material many times. Whatman filter paper No. 4, measuring 125 mm, was used to filter the entire mixture. Following its transfer into a crucible, the filtrate was dried over a water bath at 80 degrees Celsius and weighed to ensure a consistent weight (Evans, 2006).

Alkaloid determination

A 250 ml beaker containing 5 g of the sample was filled with 200 ml of 20% acetic acid in ethanol, capped, and left to stand at 250 c for 4 hours. This was filtered through No. 4 filter paper, and the filtrate was concentrated to a quarter of its initial volume in a water bath. Up until the precipitation was fully formed, concentrated ammonium hydroxide was added to the extract drop by drop. After letting the entire mixture settle, the precipitate was gathered and cleaned with diluted NH4OH (1% ammonia solution). Next, use pre-weighed filter paper to filter. After being dried at 80C in the oven, the residue on the filter paper is weighed (Evans 2006).

Tannin determination

100ml of petroleum ether was added to 5g of the crushed material in a conical flask, which was then sealed for a full day. Following filtering, the sample was let to stand for 15 minutes so that the petroleum ether may evaporate. It was then reextracted by soaking it for four hours in 100 milliliters of 10% acetic acid in ethanol. After then, the sample was filtered, and the filterate was gathered. To precipitate the alkaloids, the filtrate was mixed with 25 milliliters of NH_4OH. To get rid of part of the NH_4OH that was still in solution, the alkaloids were heated on an electric hot plate. Thirty-three milliliters were the volume left. We took 5 ml of this and mixed it with 20 ml of ethanol. Phenolphthalein was used as an indicator while titrating it with 0.1M NaOH till a pink end point is reached (Evans, 2006).

Saponin determination

After 5g of the material was weighed into a flask with 20% acetic acid in ethanol, it was left to stand for 24 hours at 500C in a water bath. This was filtered, and a water bath was used to concentrate the extract to a quarter of its initial volume. Drop by drop, concentrated NH4OH was added to the extract until the precipitate was fully formed. After letting the entire mixture settle, the precipitate was filtered out and weighed. A percentage was computed by weighing the saponin content (Evans, 2006).

Gravimetric analysis

The pre-weighed aluminum sample was subjected to a gravimetric analysis in a controlled oven at 303, 313, and 323 K with immersion times of 2, 4, and 6 hours, respectively, and 0.5 M of NaOH solution in the presence or absence of OLE inhibitor concentrations of 0.3, 0.6, and 0.9 g/L. After removing the samples from the solution, acetone-cleaning them, and reweighing, the weight loss of each sample was ascertained. Weight loss was the outcome of the weight difference, which was found using Eq. (1). Using Eqs. (2)–(4) (ASTM G1 standard) and the weight loss data gathered, the following values were computed: the corrosion rate (CR), the inhibition efficiency (I.E%), and the degree of surface covering (θ):

$$W_2 - W_1, \quad (1)$$

where W_1 is the weight before inhibition, and W_2 is the weight after inhibition

$$CR\left(\frac{cm}{hr}\right) = \frac{87600W}{A\rho t}, \quad (2)$$

where CR is the corrosion rate, w is the weight loss (g), A is the area of the coupon in (cm^2), t is time (h), and ρ is the density (g/cm^3).

$$I.E\ \% = 1 - \frac{CR_{inh}}{CR_{blank}} \times 100, \quad (3)$$

where I.E is the inhibition efficiency, with CR_{inh} and CR_{blank} corresponding to the corrosion rates in the presence and absence of inhibitors, respectively.

$$\theta = 1 - \frac{CR_{inh}}{CR_{blank}}, \quad (4)$$

where θ is the surface coverage, with CR_{inh} and CR_{blank} corresponding to the corrosion rates in the presence and absence of inhibitors, respectively.

Adsorption isotherm

The adsorption mechanism of organic inhibitors on the metal surface is described by means of adsorption isotherm investigations. According to Nwabanne et al. (2012), the adsorption isotherm model that most accurately depicts the adsorption of OLE on aluminum in 0.5 M of NaOH medium was created by fitting the inhibitor concentration (C) and the inhibitor's degree of surface coverage (θ) at 303 K for 2, 4, and 6 h immersion times into the Langmuir, Temkin, and Freundlich adsorption isotherm models expressed in linear form.

$$\frac{C_{inh}}{\theta} = \frac{1}{K_{ads}} + C_{inh} \quad (5)$$

$$\theta = K_{ads} + \ln C_{inh} \quad (6)$$

$$\text{Log } \theta = \text{Log } K_{ads} + \frac{1}{n}\text{Log } C_{inh} \quad (7)$$

Equation (8) establishes a relationship between the standard free energy of adsorption and the standard adsorption equilibrium constant of the inhibitor.

$$\Delta G_{ads} = -RT \ln(55.5K_{ads}), \quad (8)$$

where R is the gas constant (8.314KJ/mol), T is the temperature (K), and 55.5 is the standard molar of water in the solution.

FTIR analysis

At Springboard Laboratory in Awka, an Infrared Spectrophotometer from Buck Scientific was used to perform FTIR analysis on OLE and the aluminum sample in the presence of OLE inhibitors. 0.5 g of KBr were used to prepare the samples. The sample was scanned within the wave number range of 600–4000 cm−1 in order to determine the functional groups and acquire the sample's spectra wavelength.

SEM analysis

Using a scanning electron microscope, the corroded coupons were analyzed morphologically. The aluminum sample's surfaces were examined using a scanning electron microscope in both uninhibited and OLE-inhibited basic media.

Electrochemical analysis

Using a computer-controlled potentiostat/galvanostat, PDP and EIS curves were obtained in a traditional three-electrode cell. The reference electrode (RE) was Ag/AgCl in 3 M KCl, the counter electrode (CE) was platinum, and the working electrode (WE) was aluminum specimens. The WE's media-exposed area measured around 1-centimeter square. Prior to conducting potentiodynamic polarization (Tafel) studies, the electrode was left to corrode naturally for up to 12 minutes, which provided enough time for the electrode to reach a stable condition. The corrosion potential (Dcorr) of the working electrode was then found to be the steady-state OCP. Potentiodynamic measurements were conducted at 10 mVs−1 starting from the cathodic to the anodic direction (E = Dcorr ± 250 mV). Each sweep involved the employment of a new solution. The Echem Analyst software was used to analyze the PDP and EIS data. While the corrosion rate was assessed using Eq. (19), the inhibition efficiencies for PDP and EIS were computed using Eqs. (17) and (18) (Xu et al., 2017).

$$I.E\%_{PDP} = \frac{i_{corr,0} - i_{corr}}{i_{corr,0}} \times 100 \quad (9)$$

$$I.E\%_{EIS} = \frac{R_{ct} - R_{ct,0}}{R_{ct}} \times 100 \quad (10)$$

$$C.R\ (mm/yr) = 3.27 \times i_{corr} \times \frac{e}{\rho}, \quad (11)$$

where Rct and Rct,0 represent the charge transfer resistance values for aluminum in 0.5 M NaOH when the inhibitor is present and absent, respectively. The symbols icorr,0, and icorr represent the inhibited corrosion current densities, respectively. e and ρ are the equivalent weight and density of aluminum, respectively, while 3.27 is the proportionality constant.

RESULT AND DISCUSSION

An Examination of Phytochemistry

Using both qualitative and quantitative methods, phytochemical analysis of OLE produced the following phytochemicals, which are reported in (Tables 1 and 2). Phytochemicals are non-nutritive plant substances that have anti-inflammatory or disease-preventive properties. Flavonoids are secondary metabolites that are found in organic matter, such as plants and animals, and they may be beneficial to human health. Numerous antibacterial, antiviral, anti-inflammatory, anticancer, and anti-allergic properties have been demonstrated by studies on flavonoids (Kumar et al., 2021). Most oxidizing chemicals, such as singlet oxygen and different free radicals linked to a number of disorders, may be effectively scavenged by them (Naseer et al., 2018). Previous studies have demonstrated the potent immunomodulatory action of tannins (Kumar et al., 2021; Sumra et al., 2018). Wound healing is caused by alkaloids because they contain a variety of pharmacological properties, such as antibacterial and anticancer properties (Harti et al., 2016). Saponins are widely distributed in plants and are therefore considered to be phytochemical molecules that protect plants against illness (Hassan et al., 2013). The presence of these phytochemicals was thought to be responsible for the suppression of OLE-induced aluminum corrosion as the majority of them had chemical structures with heteroatoms or electron-rich linkages that made them more capable of donating electrons.

Gravimetric analysis studies

The gravimetric analysis, popularly known as the weight loss analysis was conducted on the aluminum sample in the presence and absence of orange leaf extract to

Table 1: Qualitative photochemistry result

Inhibitor	Photochemical	Photochemical	Photochemical	Photochemical
	Alkaloid	Flavonoid	Saponin	Tannin
OLE	+	++	+++	++++

Table 2: Quantitative photochemistry result.

Inhibitor	Photochemical	Photochemical	Photochemical	Photochemical
	Alkaloid	Flavonoid	Saponin	Tannin
OLE	O.679%	0.659%	1.416%	7.578%

Table 3: Gravimetric analysis using OLE

Time (h)	Inhibitor Conc. (g/L)	Wt. Difference (g)			Corrosion Rate (cm/h)			Inhibition Efficiency (%)			Degree of Surface Coverage (θ)		
		Temperature (K)			Temperature (K)			Temperature (K)			Temperature (K)		
		303	313	323	303	313	323	303	313	323	303	313	323
2	BLANK	0.032	0.032	0.037	18.62	20.58	21.85	……..	……..	……..	…….	……..	…….
	0.3	0.016	0.017	0.019	8.52	9.98	11.85	53.32	51.58	45.84	0.5221	0.5182	0.4582
	0.6	0.0042	0.0072	0.009	2.50	4.39	5.72	87.64	78.79	75.27	0.8774	0.7990	0.7428
	0.9	0.0035	0.005	0.0076	1.87	3.15	4.39	90.00	84.85	80.00	0.9000	0.8777	0.8000
4	BLANK	0.092	0.118	0.0130	28.02	36.52	40.28	……..	…….	…….	……..	……..	…….
	0.3	0.045	0.047	0.078	12.48	14.02	23.75	56.58	61.54	42.08	0.5556	0.6185	0.4102
	0.6	0.032	0.038	0.039	9.39	10.92	11.89	66.67	70.18	70.59	0.6777	0.7000	0.7255
	0.9	0.020	0.027	0.026	6.24	7.49	8.14	77.81	80.00	80.02	0.7781	0.7948	0.8000
6	BLANK	0.168	0.179	0.187	34.32	37.05	38.49	……..	……..	……..	……..	……..	…….
	0.3	0.075	0.083	0.097	15.19	16.85	19.97	55.78	54.49	49.10	0.5576	0.5555	0.4900
	0.6	0.055	0.059	0.068	10.39	12.06	13.95	69.72	68.45	63.82	0.6981	0.6742	0.6480
	0.9	0.038	0.0036	0.037	7.07	7.38	7.50	79.39	80.45	80.59	0.7948	0.8123	0.8123

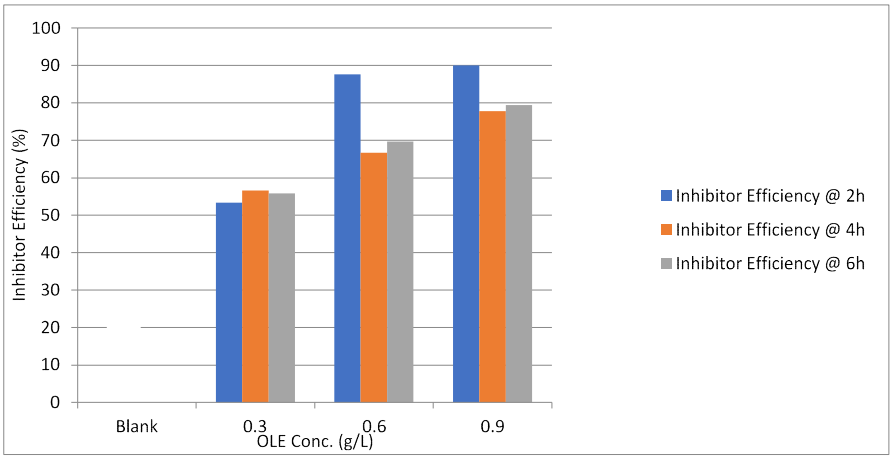

Figure 2: Effect of OLE concentration on Inhibitor efficiency using aluminium in 0.5M NaOH at a temperature of 303K

determine the weight loss, corrosion rate, surface coverage and inhibition efficiency in the basic environment.

Effect of inhibitor concentration

Table 3 displays the results of the gravimetric study, which indicate that as the concentration of Orange Leaf Extract (OLE) increases, so does the inhibition efficiency. Figure 2 illustrates this tendency. A protective coating that made it difficult for corrosive attack on the aluminum surface was created as a result of larger inhibitor molecules being absorbed at higher quantities on the aluminum surface when the concentration increased from 0.3g/L to 0.9g/L (Kolawole et al., 2019; Sani et al., 2015; Jamiu et al., 2016). In a similar vein, the outcome demonstrates that greater inhibitory efficiency is implied by large surface coverage.

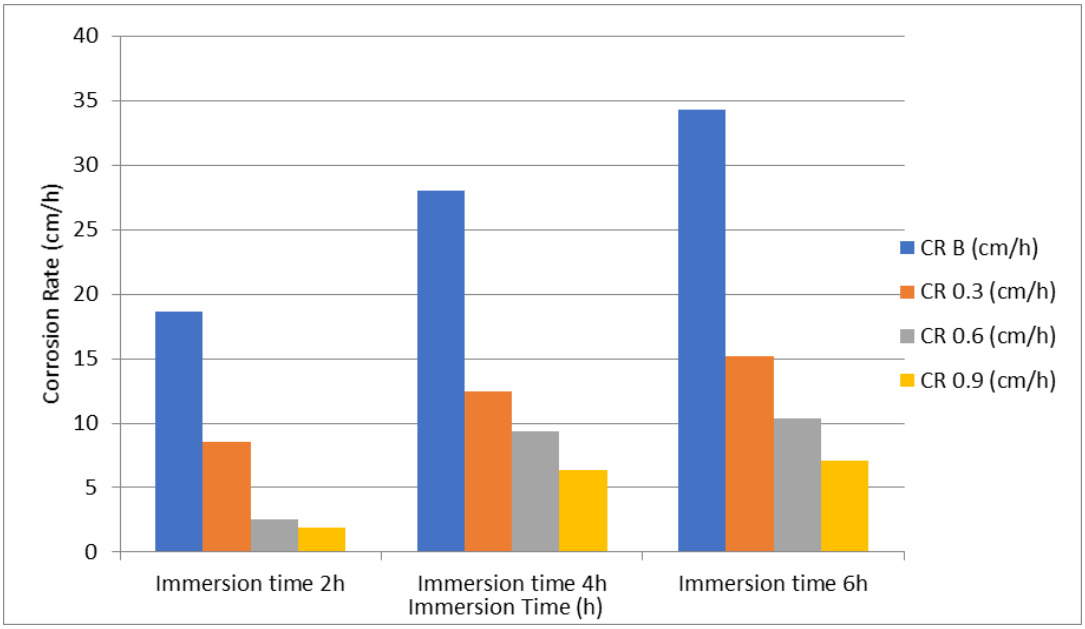

Figure 3: Effect of immersion time on OLE corrosion rate of Aluminum in 0.5 NaOH with different inhibitor concentrations at a temperature of 303K.

The inhibition efficiency was completely blank when the inhibitor was not present.

Effect of immersion time

The data in (Table 3 and Figure 3) show that a longer immersion period at different doses of OLE inhibitors resulted in a higher corrosion rate and a lower inhibition efficacy. The inhibitory efficacy was observed to be decreased as a result of the phytochemical components' desorption from the metal surface, which increased the area exposed to the corrosive attack of sodium hydroxide.

The strong inhibitory efficacy seen after immersion for two hours suggested that OLE inhibitors have been adsorbed to the aluminum surface in less than two hours. Consequently, the adsorbed effect of the inhibitor decreased with longer immersion times, whereas the mild activity of the basic media increased (Okewale and Adesina, 2020; Siaka et al., 2021; Saedah and Al-Mhyawi 2014; Moses et al., 2020). Resistance efficiency dropped as a result. Thus, inhibitor concentration is important in corrosion inhibition investigations (Kavitha et al., 2014).

Effect of temperature

The data from Table 3 show that as temperature climbed, the inhibition efficiency decreased and the rate of corrosion increased (Figures 4 and 5). This phenomenon happened because the OLE inhibitors' ability to adsorb on the aluminum surface was reduced, maybe as a result of the interacting molecules' higher average kinetic energy, which was aided by the higher temperature. Okewale and Adesina (2020) also observed that reaction rates generally increased with temperature.

Adsorption isotherm studies

The Langmuir, Freundlich, and Temkin adsorption isotherm models were fitted to the experimental data. The adsorption isotherm fitting outcomes are displayed in (Figures 6–8,) while (Table 4), displays the adsorption isotherm parameters that were determined. With a correlation value (R2) of 0.947, the Temkin isotherm outperformed Freundlich and Langmuir in terms of fit for OLE inhibitors, according to the findings. The R2 values were nearly one, and the graphs showed good linearity. This suggests that the Temkin adsorption isotherm is strongly adhered to by the OLE inhibitors. According to the Temkin isotherm model, adsorption is characterized by a uniform distribution of binding energies up to a maximum binding energy, and the adsorption heat of every molecule present in the OLE decreases linearly with an increase in the coverage of the adsorbent surface (Piccin et al., 2011). According to the Temkin adsorption isotherm model, when the surface coverage of the adsorbent increases, the adsorption heat of the OLE molecules reduces linearly. This can be seen in (Figures 6, 7 and 8), where the surface coverage increases from 0.52 to 0.88 to 0.90. Accordingly, the adsorption mechanism of the inhibitors on Aluminum in NaOH media is typical of physical adsorption, which involves electrostatic interaction between charged molecules. This is demonstrated by the adsorption of OLE inhibitors on

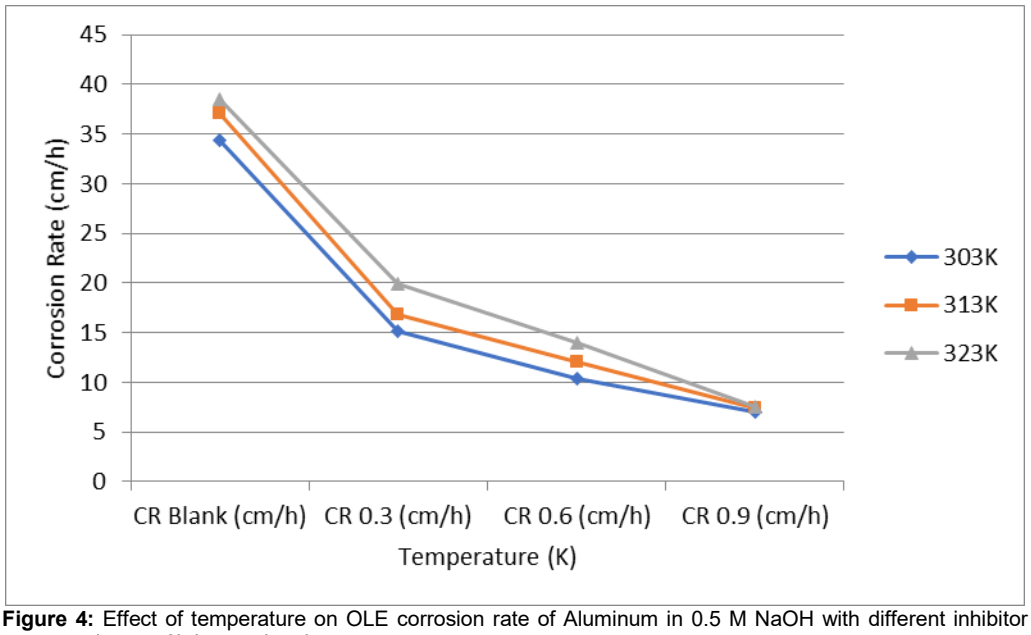

Figure 4: Effect of temperature on OLE corrosion rate of Aluminum in 0.5 M NaOH with different inhibitor concentrations at 6h immersion time.

Table 4: Adsorption Isotherm Parameters for OLE.

Isotherm Models	Parameters	Inhibitor OLE
Langmuir	Intercept	0.49333
	Slope	0.5
	R^2	0.83678
	G_{ads}(kJ/mol)	-12.700
	R_L	0.2740
Freundich	Intercept	0.00884
	Slope	0.52103
	R^2	0.94616
	G_{ads}(kJ/mol)	12.380
Temkin	Intercept	0.98969
	Slope	0.36761
	R^2	0.94784
	G_{ads}(kJ/mol)	-9.205

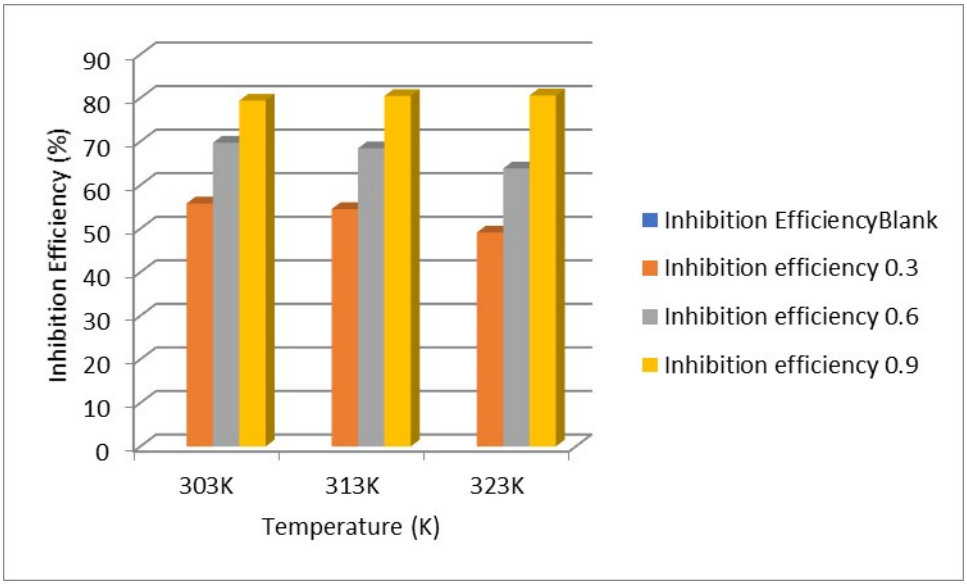

Figure 5: Effect of temperature on Inhibition efficiency of Aluminum in 0.5 M NaOH with different inhibitor concentrations at 6h immersion time

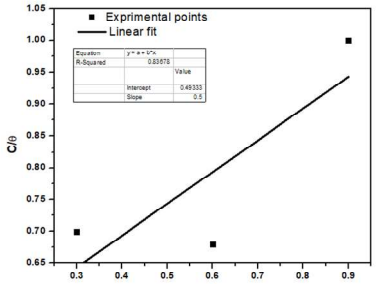

Figure 6: Langmuir Isotherm Model of OLE

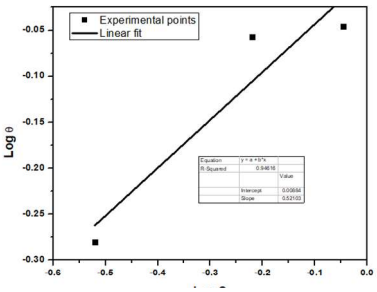

Figure 7: Freundlich Isotherm model of OLE

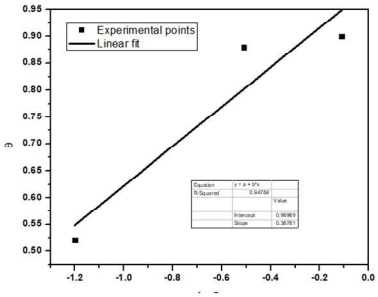

Figure 8: Temkin Isotherm model of OLE

Table 5: EDX analysis

Element Name	Element Number	Atomic Concentration (ppm)	Weight concentration (ppm)
Carbon	6	88.96	85.86
Nitrogen	7	0.24	0.52
Sodium	11	0.93	1.72
Aluminum	13	9.20	10.36
Magnesium	12	0.24	0.46
Silicon	14	0.17	0.38
Chlorine	17	0.10	0.30
Phosphorous	15	0.09	0.21
Sulfur	16	0.07	0.19
Calcium	20	0.00	0.00
Potassium	19	0.00	0.00
Titanium	22	0.00	0.00
Iron	26	0.00	0.00
	Total	100	100

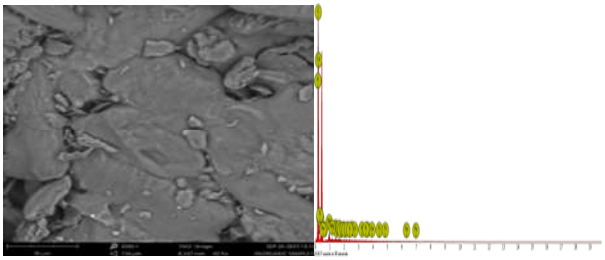

Figure 9: SEM-EDX Blank Aluminum Metal

the surface of Aluminum at the studied temperature with different immersion times (Amoo et al., 2019).

SEM analysis

One useful method for characterizing the structure and composition of materials is SEM-EDX analysis. Scanning electron microscopy (SEM) in this study focuses on the sample's surface morphology, whereas electron dispersive X-ray spectroscopy (EDX) identifies the elements and their specific numbers, atomic concentrations, and weight concentrations.

SEM interpretation of blank aluminum

Eleven elements were identified through EDX analysis of blank aluminum metal, along with their individual element numbers, atomic concentrations (ppm), and weight concentrations (ppm), respectively. The morphology of the SEM image, observed in blank aluminum metal prior to corrosion inhibition, shows a distinctive irregular shape with a large parchment covering almost the surface area of the material with gray background (Figure 9). The sample has a 100-ppm atomic concentration of elements with carbon as the major element and a 100-ppm weight concentration of elements with aluminum as the predominant element, according to an EDX examination of blank aluminum metal (Table 5).

SEM interpretation of aluminum metal after inhibition

The morphology of the SEM image of the aluminum

Table 6: EDX analysis

Element Name	Element Number	Atomic concentration (ppm)	Weight concentration (ppm)
Carbon	6	84.66	81.33
Nitrogen	7	14.12	15.82
Aluminum	13	0.39	0.83
Sodium	11	0.26	0.48
Iron	26	0.07	0.31
Magnesium	12	0.15	0.28
Silicon	14	0.10	0.22
Phosphorous	15	0.09	0.22
Sulphur	16	0.08	0.20
Chlorine	17	0.04	0.13
Calcium	20	0.03	0.09
Potassium	19	0.03	0.08
	Total	100.02	99.99

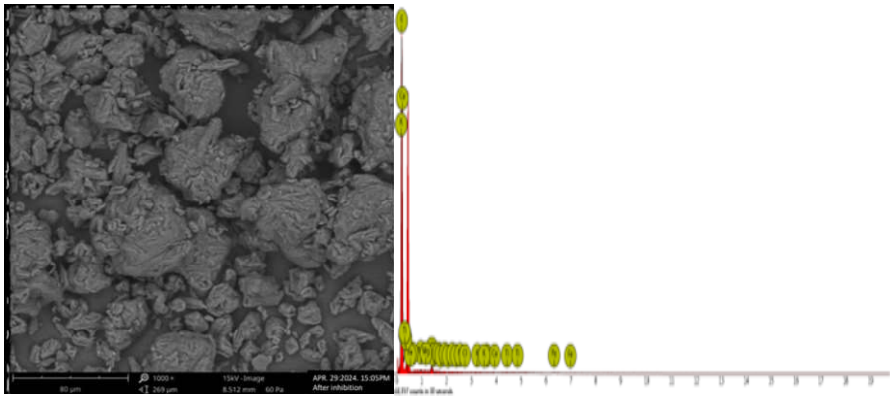

Figure 10: SEM-EDX aluminum metal after inhibition

metal after inhibition displays a big, distinctive, irregularly shaped cut across the material's surface against a dark backdrop, indicating the presence of active sites for the inhibition of corrosion with orange leaf extract (Table 6 and Figure 10). Twelve elements were found in Aluminum Metal After Inhibition by EDX analysis, along with information on each element's unique element number, atomic concentration (ppm), and weight concentration (ppm), respectively. Following inhibition, an EDX analysis of aluminum metal reveals that the sample has an atomic concentration of 100.02 ppm and a weight concentration of 99.99 ppm, with the elements carbon and nitrogen predominating.

Fourier transform infrared (FTIR) analysis

An analytical method called Fourier Transform Infrared (FTIR) (Figure 11) is used to examine organic functional groups and other substances that are present in a sample. In the current work, functional groups in the aluminum blank utilized for the corrosion inhibition investigation with extracted orange leaf extract were examined using Fourier transform infrared spectroscopy (FTIR) (Xiuli et al., 2021). The peak values near 1886.6046cm-1, 1021.908cm^{-1}, and 1287.643cm^{-1} in the FTIR (Table 7) were attributed to the ester compound's C0 stretching vibration, respectively. Spectral height of approximately 1441.593cm^{-1} was attributed to the alkene compound's C=C anti-symmetric vibration. The N-H stretching vibration of the 10-amine compound was allocated to the medium band around 1603.565cm^{-1} and 1874.017cm^{-1}, respectively. The peak height, which is approximately 1985.955 cm^{-1}, is associated with the thiol compound's S-H stretching vibration. A wavelength of approximately 2109.152cm^{-1} was attributed to the carboxylic acid compound's C00 stretching vibration. The stretching vibration of CN in the nitrile compound was attributed to the highest value at approximately 2509.072cm^{-1}. The C-H stretching vibration of the methylene molecule was identified as the source of the weak bands at 2688.576cm-1, 2798.775cm^{-1}, and 2976.341cm^{-1}, in that order. Strong bands were linked to the 0H stretching vibration of 20 and 30 alcoholic compounds, respectively, at 3134.419cm^{-1}, 3340.212cm^{-1}, 3526.961cm^{-1}, and 3808.158cm^{-1}. Based on the findings in (Table 8 and Figure 12), the absorbance at 1328.800cm^{-1} was attributed to the alkene compound's C=C anti-symmetric vibration. The N-H stretching vibrations of amine compounds 10 and 20 were allocated to the medium band around 1633.799cm-1, 1883.620cm^{-1}, and 3456.369cm^{-1}, respectively. The wavelength around 2197.752cm-1 was assigned to the C0 anti-symmetric vibration of the carbonyl compound, while the peak centered around 2058.408cm-1 was assigned to the

Table 7: FTIR Interpretation of blank aluminum metal before corrosion inhibition with OLE.

Wavelength (cm^{-1})	Functional group	Compounds
886.6046	R-0-R	Ether C0 symmetric strech
1021.908	R-0-R	Ether C0 symmetric strech
1287.643	R-0-R	Ether C0 symmetric strech
1441.593	H_2C=CH	Ethene C=C anti-symmetric stretch
1603.565	RNH_3	1^0 amine NH stretch
1874.017	RNH_3	1^0 amine NH stretch
1985.955	SH	Thiol S-H symmetric stretch
2109.152	RC00H	Carboxylic acid C00 stretching vibration
2509.072	R-C≡N	Nitriles CN anti-symmetric stretch
2688.576	CH_2	Methylene CH symmetric stretch
2798.775	CH_2	Methylene CH symmetric stretch
2972.926	CH_2	Methylene CH symmetric stretch
3134.419	R_2CH0H	2^0 alcohol 0H symmetric stretch
3340.212	R_3CH0H	3^0 alcohol 0H symmetric stretch
3526.961	R_3CH0H	3^0 alcohol 0H symmetric stretch
3808.158	R_3CH0H	3^0 alcohol 0H symmetric stretch

Table 8: FTIR interpretation of aluminum metal after corrosion inhibition with OLE.

	Functional group	Compounds
1328.800	H_2C=CH	Ethene C=C anti-symmetric stretch
1633.799	RNH_3	1^0 amine NH stretch
1883.620	RNH_3	1^0 amine NH stretch
2058.408	RC00H	Carboxylic acid C00 stretching vibration
2197.752	RC=0	Carbonyl compound C0 anti-symmetric stretch
2449.141	R-C≡N	Nitriles CN anti-symmetric stretch
2695.664	CH_2	Methylene CH symmetric stretch
2860.605	CH_2	Methylene CH symmetric stretch
2939.934	CH_2	Methylene CH symmetric stretch
3100.05	R_2CH0H	2^0 alcohol 0H symmetric stretch
3230.311	R_2CH0H	2^0 alcohol 0H symmetric stretch
3456.369	R_2NH	2^0 amine NH stretch
3680.621	R_3CH0H	2^0 alcohol 0H symmetric stretch
3827.368	R_3CH0H	3^0 alcohol 0H symmetric stretch

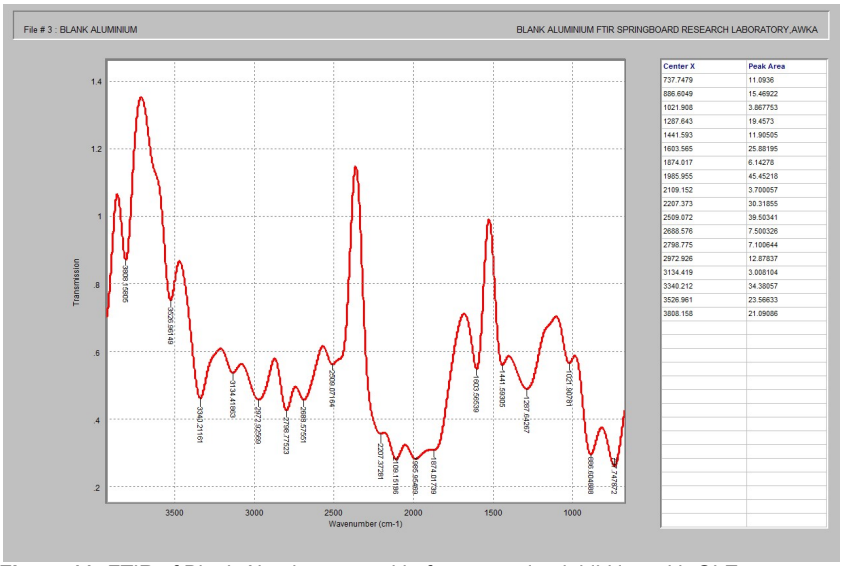

Figure 11: FTIR of Blank Aluminum metal before corrosion inhibition with OLE

C00 stretching vibration of the carboxylic acid compound. The peak value of 2449.141cm-1 was attributed to the nitrile compound's CN stretching vibration. The weak bands around 2695.664cm^{-1}, 2860.605cm^{-1}, and 2939.934cm^{-1} were identified as the methylene compound's C-H stretching vibrations, in that order.

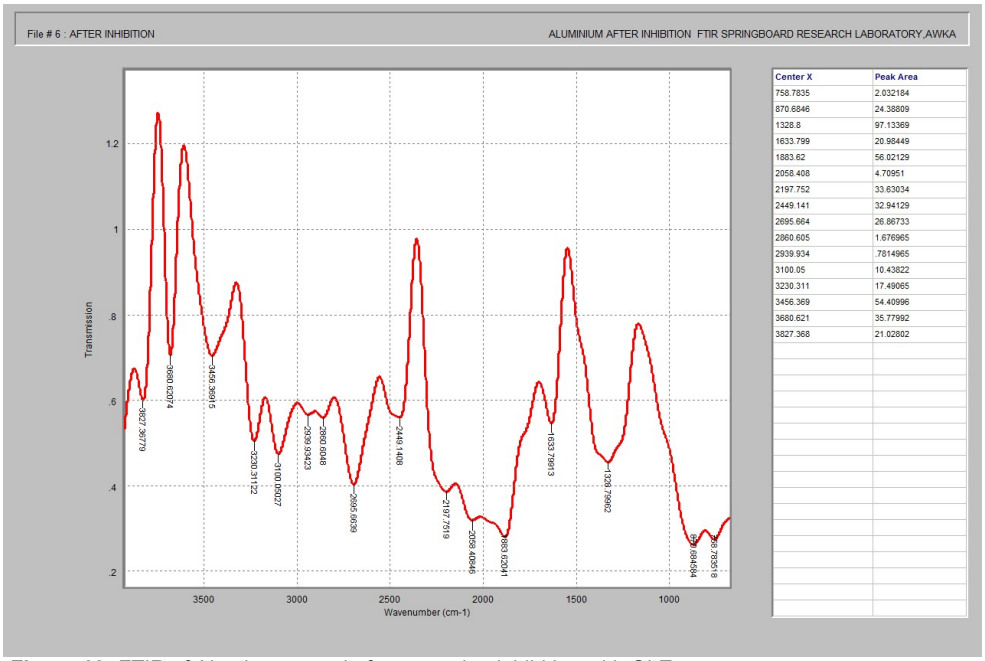

Center X	Peak Area
758.7835	2.032184
870.6846	24.38809
1328.8	97.13369
1633.799	20.98449
1883.62	56.02129
2058.408	4.70951
2197.752	33.63034
2449.141	32.94129
2695.664	26.86733
2860.605	1.676965
2939.934	.7814965
3100.05	10.43822
3230.311	17.49065
3456.369	54.40996
3680.621	35.77992
3827.368	21.02802

Figure 12: FTIR of Aluminum metal after corrosion inhibition with OLE

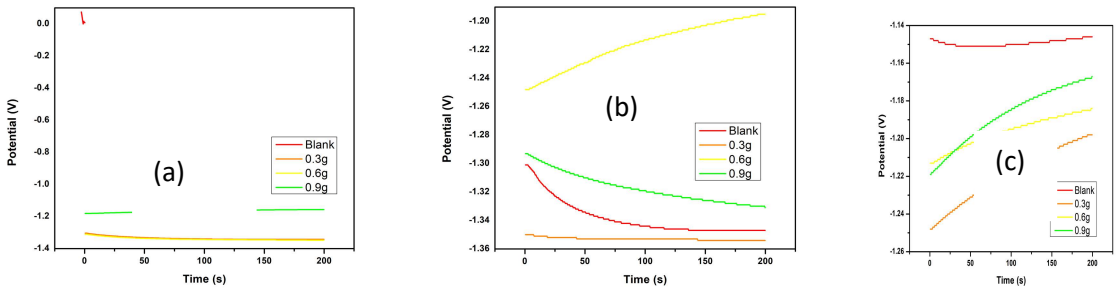

Figure 13: OCP curve for Aluminum in 0.5 NaOH OLE inhibitor at 303K for (a) 2h (b) 4h (c) 6h Immersion times

Strong bands at 3680.621cm-1, 3827.368cm^{-1}, and 3100.05cm^{-1} were identified as the 0H stretching vibrations of alcohol compounds 10 and 30, respectively.

Electrochemical measurement studies

Open-circuit potential (OCP)

The potential created between the environment and the working electrode, which is the metallic surface under study, in relation to a reference electrode that will be put into the electrolyte near the working electrode, is known as the open circuit potential. The collected results showed that before the impedance and polarization experiments started, the solutions under investigation had acquired a satisfactory level of stability. The OCP value first varied at each concentration of OLE inhibitors before stabilizing (Figure 13). The value of OCP increased in tandem with an increase in OLE concentrations. However, when the aluminum was added to 0.3 g/L of the OLE inhibitor, there was a discernible fluctuation that shifted in a negative direction throughout the course of the time. The value of OCP remained stable and was trending upward at OLE inhibitor concentrations of 0.6 and 0.9 g/L. This movement points to an OLE inhibitor's mixed-type corrosion inhibition action (Solomon et al., 2020). The OLE molecules' steady and unstable adsorption on the aluminum sample's surface could be the cause of the behavioral abnormalities. The adsorption isotherm, which demonstrates that it is also fitted to the Temkin isotherm model, is confirmed by this assertion of OLE molecules (Figure 13 a,b,c).

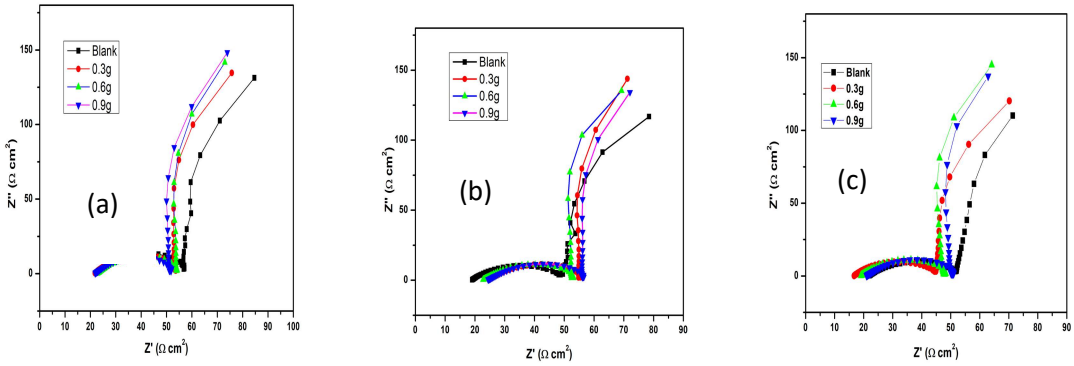

Figures 14 (a,b,c) Nyquist plots of Aluminum in 0.5M NaOH in the Absence and presence of different concentrations of OLE inhibitor at different immersion times.

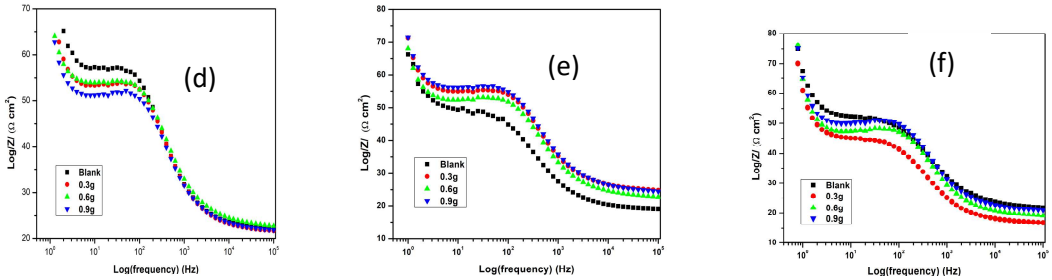

Figures 14 (d,e,f) Bode plots of Aluminum in 0.5M NaOH in the Absence and presence of different concentrations of OLE inhibitor at different immersion times**.**

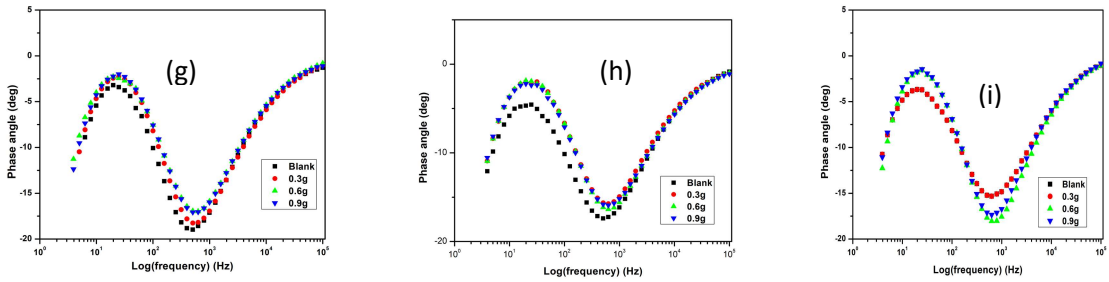

Figures14 (g,h,i) Phase plots of Aluminum in 0.5M NaOH in the Absence and presence of different concentrations of OLE inhibitor at different immersion times.

Electrochemical Impedance Spectroscopy (EIS)

With their corresponding Bode and phase angle representations displayed in (Figures 14: d, e, f) and (Figures 14: g, h, i), the Nyquist electrochemical plot of aluminum in 0.5M NaOH solution is shown in (Figures 14: a, b, and c) in the presence and absence of increasing concentrations of OLE inhibitors at different immersion times. A similar semi-circle with a single, incomplete capacitive loop may be seen in the Nyquist plots of OLE inhibitors, suggesting a corrosion process controlled by charge transfer (Solomon et al., 2020). While the imperfections were brought about by various physical phenomena like roughness and heterogeneities on the working electrode surface, which could result from a corrosive attack on exposure to the acid solution, impurities, grain boundaries, and distribution of the surface-active sites, the shapes were similar because the corrosion mechanism remained unchanged (Solomon et al., 2020). The Nyquist plot width rose with the addition of OLE inhibitor at all doses, but this increase was most pronounced at 0.9 g/L for the inhibitor during all immersion times, indicating that the OLE inhibitor gave the aluminum greater corrosion resistance. The inhibitor's phase angle and Bode modulus graphs likewise showed this effect (Chukwunyere and Egbosiuba, 2023).

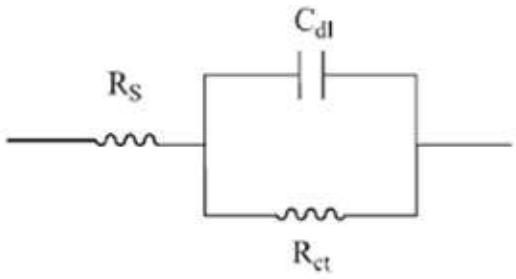

Rs = Rp, Rct=Ru, Cd=Cs CPE fitting

Figure 15: The equivalent circuit diagram was employed to suit the data on impedance.

Table 9: Aluminum's electrochemical impedance characteristics in a 0.5M NaOH solution with and without an OLE inhibitor at various immersion durations.

R_S (Ωcm^2)	R_{ct} (Ωcm^2)	n_1 (Ω)	Y_{01} ($\Omega^{-1}s^2cm^{-2}$)	R_f (Ωcm^2)	n_2 (Ω)	Y_{02} ($\Omega^{-1}s^2cm^{-2}$)	L (H)	IE (%)	C_{dl} (μFcm^{-2})
2 Hours									
33.81	23.8	0.925	1.33×10^{-5}	2.17×10^{-6}	0.457	2.83×10^{-7}	1.13×10^{-2}		6.31×10^{-6}
377.2	29.33	0.957	2.18×10^{-5}	1.137	0.964	2.26×10^{-3}	8.43×10^{-5}	18.85	1.286×10^{-5}
404	30.94	0.900	2.74×10^{-5}	2.804	1.00	2.78×10^{-3}	6.94×10^{-7}	23.08	7.78×10^{-6}
407.6	31.56	0.810	2.59×10^{-5}	3.221	1.00	2.69×10^{-3}	7.89×10^{-4}	24.58	2.56×10^{-6}
4 Hours									
446.2	18.44	0.913	2.78×10^{-5}	2.29×10^{-2}	2.47×10^{-2}	2.80×10^{-3}	9.75×10^{-2}		9.48×10^{-6}
28.53	20.64	0.920	3.52×10^{-5}	1.384	7.52×10^{-1}	1.62×10^{-5}	2.10×10^{-3}	10.66	1.218×10^{-7}
430.9	31.06	0.931	2.87×10^{-5}	1.000	7.31×10^{-1}	2.91×10^{-3}	2.73×10^{-3}	40.63	1.698×10^{-5}
437.7	38.98	0.915	2.92×10^{-5}	8.615	7.46×10^{-1}	2.89×10^{-3}	2.62×10^{-3}	52.69	1.023×10^{-5}
6 Hours									
28.05	23.73	0.930	3.10×10^{-7}	1.829	0.897	1.28×10^{-5}	4.58×10^{-6}		1.219×10^{-7}
26.31	28.16	0.938	3.32×10^{-7}	0.866	0.667	1.57×10^{-5}	8.36×10^{-5}	15.73	1.748×10^{-5}
434.5	30.36	0.901	2.68×10^{-5}	1.88	0.772	2.83×10^{-3}	9.97×10^{-10}	21.84	7.75×10^{-6}
437.7	35.78	0.960	2.87×10^{-5}	0.011	0.804	2.95×10^{-3}	5.10×10^{-7}	33.68	2.14×10^{-5}

With increasing quantities of OLE and inhibitor, the phase angle was shown to be more negatively oriented, while the Bode modulus shifted in a noble direction. It may be inferred that the adsorption of OLE molecules on the aluminum surface slowed down the rate of charge transfer in the OLE inhibited system, reinforcing the protective barrier (Solomon et al., 2020).

Figure 15, displays the equivalent circuit that was utilized to fit the impedance values. The solution resistance (Rs) in the equivalent circuit is denoted by Rs, the charge transfer resistance (Rct) by Rf, the resistance of the adsorbed film's outer layer is described by Rf, and the constant phase element (CPE) of the inner and outer film layers (Y01 and Y02, respectively) by n1 and n2. Brug's formula (Brug et al., 1984) can be used to compute the double-layer capacitance (Cdl) for a non-ideally polarized electrode, when charge transfer governs the corrosion process and diffusion is not taken into account.

$$C_{dl} = Y_0^{1/n}\left(\frac{1}{R_s} + \frac{1}{R_{ct}}\right)^{n-1/n} \quad (12)$$

Tables 9 and 10 contain all of the derived values and calculated parameters. Based on the tables, an increase in OLE inhibitor concentration led to a corresponding rise in Rct values, which in turn produced an increase in inhibitor efficiency. Furthermore, for every immersion time under study, the Cdl values dropped. According to Ameh et al. (2016), the higher Rct values further supported the theory that the slower rate of aluminum corrosion was to blame.

Electrochemical measurements

Polarization via potentiodynamics Electrochemical impedance and PDP Using a computer-controlled potentiostat/galvanostat, three conventional electrodes were used to construct spectroscopic EIS curves. The electrolyte resistance (Rs), the capacitance double layer (Cd), and the charge transfer resistance (Rct) are all measured using the EIS approach. Ag/AgCl in 3M KCl electrolyte was utilized as the reference electrode (RE), platinum electrode as the counter electrode (CE), and the sample as the working electrode (WE). The WE's exposed surface area to the media was roughly 1 cm2. When the medium was allowed to reach a stable

Table 10: Potentiodynamic polarization parameters of Aluminum in 0.5 M NaOH solution without and with different concentrations of OLE inhibitor at 313 K at 2, 4, and 6 h.

Inh. Con. (g/L)	E_{corr} (mV/SCE)	i_{corr} ($mAcm^{-2}$)	β_a ($mVdec^{-1}$)	$-\beta_c$ ($mVdec^{-1}$)	CR (cm/hr)	η (%)	θ
2 Hours							
Blank	-1.130	6.965×10^{-3}	406×10^{-3}	332.2×10^{-3}	1960		
0.3	-507.0	1.560×10^{-3}	215×10^{-3}	211.8×10^{-3}	712.9	63.38	0.6338
0.6	-508.0	1.25×10^{-3}	854.9×10^{-3}	738.5×10^{-3}	3771	82.02	0.8208
0.9	-495.0	1.15×10^{-3}	40×10^{-3}	42.20×10^{-3}	109.9	83.48	0.8348
4 Hours							
Blank	-1.340	8.67×10^{-3}	979.9×10^{-3}	593.7×10^{-3}	3.963×10^{-3}		
0.3	-1.350	1.250×10^{-3}	162.7×10^{-3}	123.6×10^{-3}	573.3	86	0.86
0.6	-1.330	1.140×10^{-3}	49.20×10^{-3}	44.60×10^{-3}	107.3	86.85	0.8685
0.9	-1.350	0.59×10^{-3}	568.1×10^{-3}	485.1×10^{-3}	2099	93	0.93
6 Hours							
Blank	-1.190	19.80×10^{-3}	395.1×10^{-3}	296.4×10^{-3}	9035		
0.3	-1.340	372×10^{-6}	52.20×10^{-3}	54.9×10^{-3}	124.2	98	0.98
0.6	-1.350	281×10^{-6}	41.60×10^{-3}	43.60×10^{-3}	82.83	98.50	0.9850
0.9	-1.160	260×10^{-6}	1.160	318.7×10^{-3}	2779	98.98	0.9898

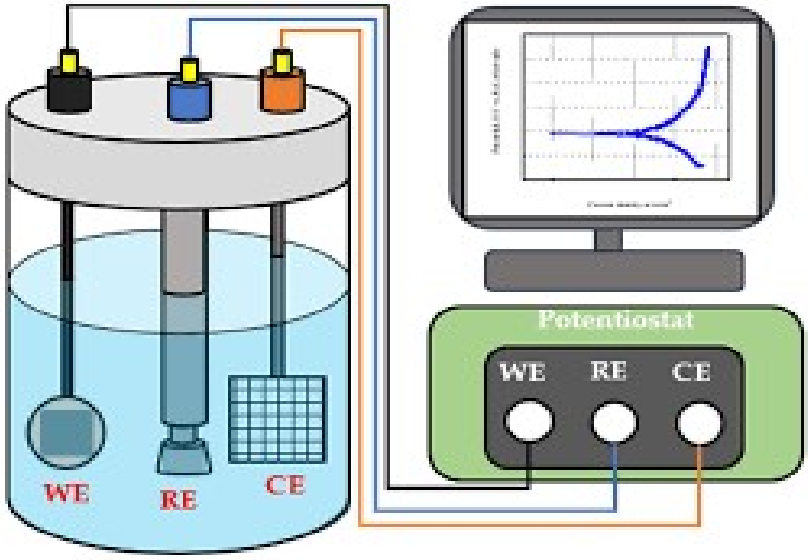

Figure 16: Electrochemical corrosion cell setup

condition at a constant open circuit potential without current flow, the sequential approaches were employed for the study. The AC signal is then scanned across a broad frequency range of 0.1 HZ to 10 KHZ to produce an impedance spectrum and to monitor the potentiodynamic polarization curve for the electrochemical cell that is being tested.

Potentiodynamic polarization (PDP)

In order to learn more about the kinetics of aluminum's anodic and cathodic processes, polarization experiments were carried out at 313 K for immersion times ranging from 2 to 6 hours in 0.5 M NaOH, both with and without OLE inhibitor. Figure 16 shows the aluminum polarization curves at various OLE inhibitor doses and immersion periods. After analyzing the polarization curve, the appropriate parameters were determined through extrapolation, which included the corrosion potential (Ecorr), corrosion current density (icorr), and the anodic (βa) and cathodic (βc) Tafel slopes (Chukwunyere and Egbosiuba, 2023). The inhibition efficiency (η%) and corrosion rates of OLE inhibitor were calculated using equations 9 and 10, and the results are shown in (Table 10).The polarization curve demonstrates that the addition of OLE inhibitor repressed both the anodic and cathodic reactions, suggesting that OLE function as mixed-type inhibitors to inhibit the anodic dissolution and cathodic hydrogen evolution events (Figure 17). Table 10 shows that the addition of OLE inhibitor with the highest displacement at 6 hours of immersion time resulted in a corrosion potential (Ecorr) of 15 mV as compared to the

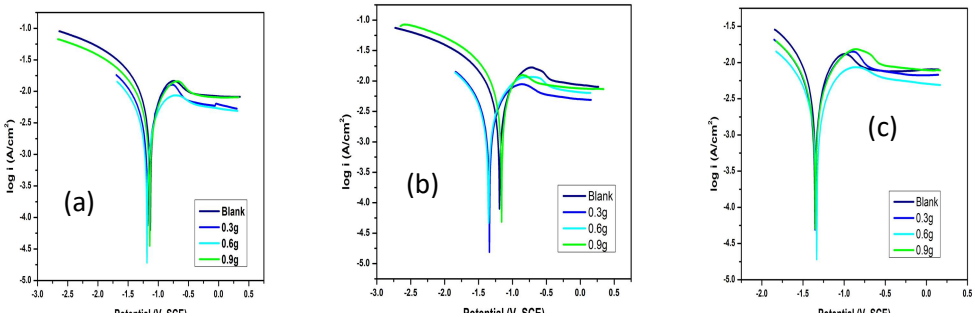

Figure 17: Polarization curves of Aluminum in 0.5 M NaOH with different concentrations of OLE inhibitor at 303 K for (a) 2h (b) 4h (c) 6h immersion time

blank acid solution. The fact that the Ecorr value is less than 85 mV indicates that OLE inhibitors function as mixed-type inhibitors, regulating the anode and cathode's corrosion reaction (Xanxia et al., 2022). Additionally, the values of the corrosion potential and corrosion current density gradually decrease as the inhibitor concentration rises. As a result, the anodic and cathodic inhibition performances block the active sites on the aluminum surface, increasing inhibition efficiency and lowering corrosion rates (Thesis, 2009). The OLE molecules were adsorbed by the aluminum during all immersion times, resulting in this effect. With an inhibitor concentration of 0.9 g/L, the OLE's inhibition efficiency peaked at 6 hours of immersion time, or 98.98%. The same table demonstrate that for both inhibitors, the change in the anodic Tafel slope (βa) is greater than the shift in the cathodic Tafel slope (βc) when compared to the blank. This suggests that the anodic reaction is mostly affected by OLE inhibitors (Chukwunyere and Egbosiuba, 2023).

Conclusion

The study revealed that OLE contains phenolic agents, metabolites, alkaloids, flavonoids, saponin, and tannin which inhibit corrosion by creating a barrier on aluminum surfaces. Gravimetric analysis showed that inhibition efficacy increased with OLE concentration but decreased with higher temperatures and longer exposure times. The highest inhibition efficiency of 90% was observed at an OLE concentration of 0.9 g/L for 2 hours at 303 K, indicating that aluminum corrosion in NaOH is influenced by temperature, concentration, and immersion period. These findings offer valuable insights for understanding and controlling aluminum corrosion in specific environments. The Temkin adsorption isotherm model supports the OLE inhibitor's physisorption on aluminum, as indicated by the negative ΔGºads, suggesting effective corrosion inhibition. The OLE inhibitor shows increased half-life and decreased rate constant, further confirming its efficacy. FTIR analysis revealed active inhibition-contributing functional groups in OLE. SEM analysis demonstrated the formation of a protective coating, effectively mitigating corrosion on aluminum surfaces due to phenolic agent/metabolite adsorption. The investigation of the OLE inhibitor's impact on corrosion revealed significant results from various spectroscopic and electrochemical analyses. The findings show that the corrosion process is mainly influenced by charge transfer. Higher inhibitor concentrations led to increased efficiency, indicating a direct correlation between inhibitor concentration and metal surface adhesion. The OLE inhibitor demonstrated an impressive 93% corrosion inhibition efficiency at a 4-hour immersion duration. It was also found to disrupt both anodic and cathodic processes, exhibiting promising potential in mitigating corrosion at multiple stages.

REFERENCES

Adegbite, J. A., Sanni, L. O., Osinowo, O. A. (2006). *Comparative evaluation of chemical and sensory properties of Achatina achantina and Archachatina marginata. International Journal*. Asset Series A, 6 (2):1–6.

Aiawadhi, K., Robinson, M., Chalmers, A., Winning, I. G. (2008). *Inhibition of weld corrosion in flowing brines containing carbon dioxide. NACE* - International Corrosion Conference Series, 086221–0862214.

Ameh P.O, Ukoha P, Ejikeme P, Eddy NO (2016). *Thermodynamic, Chemical and Electrochemical Investigations of 4-Hydrobenzoic Acid as Corrosion Inhibitor for Mild Steel Corrosion in Hydrochloric Acid Solutions*. Ind Chem 2: 119. DOI: https://doi.org/10.4172/2469-9764.1000119

Ashraf, A., Sarfraz, R.A., Rashid, M.A., Mahmood, A., Shahid, M. Noor, N. (2016). *Chemical composition, antioxidant, antitumor, anticancer, and cytotoxic effects of Psidium guajava leaf extracts*. Pharm. Biol. 2016, 54, 1971–1981.

Boffarh B.P.(2003). *Corrosion Inhibitors in the Water Treatment Industry in ASM Handbook*, Vol 13A, ASM International; Materials Park OH..

Brug, G.J., van den Eeden, A.L.G., Sluyters-Rehbach, M., Sluyters, J.H. (1984). *The analysis of electrode impedances is complicated by the presence of a constant phase element. J. Electroanal. Chem.* 176, 275–295, 1984. Https://doi.org/10.1016/S0022-0728(84)80324-1.

Chen, H.Y.; Yen, G.C.(2009). *Antioxidant activity and free radical-scavenging capacity of extracts from guava (Psidium guajava L.) Leaves.* Food Chem. 2007, 101, 686–694.

Chukwunyere and Egbosiuba, I. E. and Egbosiuba, T.C. (2023). Investigation of the corrosion inhibition performance of snail slime on the exposed surface of mild steel in acidic environment. https://doi.org/10.1016/j.clce.2023.100114.

Evans, W.C., (2006). *Pharmacognosy,* 16th Edition, W.B. Sounders, USA. Pp. 243-283.

Farag, R.S.; Abdel-Latif, M.S.; Abd El Baky, H.H.; Tawfeek, L.S.(2020). *Phytochemical screening and antioxidant activity of some medicinal plants' crude juices.* Biotechnol. Rep. 2020, 28, e00536.

Fontana M.G, Greener N.D, (1978). *The Eight Forms of Corrosion, Corrosion Engineering*, MG-Graw-Hill, New York.

Frank N.K, and John MC, (1979). *The Nalco Water Handbook*.

Harti, A.S, Sulisetyawati, D., Murharyati, A., Oktariani, M. (2016). *The Effectiveness of Snail Slime and Chitosan in Wound Healing, International Journal of Pharma Medicine and Biological Sciences, 5: 1–5.*

Hassan SB, Gulbo J, Hu K, Berenjian S, Morein B, Nygren P. (2013). *The Nanoparticle Quillaja Saponin BBE is selectivity active towards renal cell carcinoma.* Anticancer Res 2013;33(1):143-51

Izionworu, V. O., Ukpaka, C. P., & Oguzie, E. (2020). *Green and eco-benign corrosion inhibition agents Alternatives and options to chemical-based toxic corrosion inhibitors Green and eco-benign corrosion inhibition agents: Alternatives and options to chemical-based toxic corrosion inhibitors.* Https://doi.org/10.5281/zenodo.3706592.

Jamiu K., Odusote, David O., Owalude, Sunday J., Olusegun, & Raheem A. Yahya, (2016). *Inhibition Efficiency of Moringa oleifera Leaf extracts on the Corrosion of Reinforced Steel Bar in Hcl Solution*. The West India J. Of Engineering. 38(2):6470.

Jiang, L.; Lu, J.; Qin, Y.; Jiang, W.; Wang, Y. (2020). *Antitumor effect of guava leaves on lung cancer: A network pharmacology study*. Arab. J. Chem. 2020, 13, 7773–7797.

Kavitha N., Manjula P., & Anandha kumar N., (2014). *Synergistic Effect of Papaya Leaves Extract Zn^{2+} in Corrosion Inhibition of Mild Steel in Aqueous Medium*. Research Journal of Chemical Sciences. 4(8):88–93.

Kolawole S. Amoo, Jacob S. Jatau, M. Abdulwahab (2019). *Corrosion Inhibitive Effect of Psidium Guajava Leaves on Mild Steel in an Induced Alkaline Solution*. Journal of Scientific and Engineering Research, 2019, 6(6):116-127.

Kumar, V. K.P., Narayanan Pillai Sankara M., & Rexin Thusnavis G., (2021). *Inhibition of Mild Steel Corrosion in Hydrochloric* Ac2nd Ed, John Wiley & Sons, New York.

Leelavathi S., & Rajalakshmi R., (2013). *Dodonaea viscose (L.) Leaves Extract as an acid Corrosion Inhibitor for Mild Steel.* Journal of Material and Environment Science. Vol. 4(5), pp 625–638.

Miralrio, A., & Vázquez, A. E. (2020). *Plant extracts as green corrosion inhibitors for different metal surfaces and corrosive media*: A review. Processes, *8*(8). Https://doi.org/10.3390/PR8080942

Moses M. Solomon, Saviour A. Umoren, Mumtaz A. Quraishi, Divya B. Tripathy, Ekaette J. Abai. (2020). *Effect of alkyl chain length, flow, and temperature on the corrosion inhibition of carbon steel in a simulated acidizing environment by an imidazoline-based inhibitor*. Journal of Petroleum Science and Engineering 187 (2020) 106801. Https://doi.org/10.1016/j.petrol.2019.106801

Nwabanne, J. T., Okafor, V. N. (2012). *Adsorption and thermodynamics study of the inhibition of corrosion of mild steel in H_2SO_4 medium using Vernonia amygdalina, J. Minerals Mater*. Characteri. Eng., 11, (2012), 885-890.

Okewale, A.O; Adesina, O.A. (2020). *Kinetics and Thermodynamic Study of Corrosion Inhibition of Mild Steel in 1.5M HCl Medium using Cocoa Leaf Extract as Inhibitor*. J. Appl. Sci. Environ. Manage. Vol. 24 (1) 37-47 January 2020. DOI: https://dx.doi.org/10.4314/jasem.v24i1.6

Piccin J.S, Dotto G.L. and Pinto L.A.A (2011). *Adsorption Isotherm and Thermochemical Data of FD&C Red N◦40 Binding* By Chitosan.

Priya Bhardwaj, (2017). *"studies on potential green corrosion inhibitors for mild steel in different media."*

Putilora I, Balezin S, Barannik V, (1960). *Metalic Corrosion Inhibitors, G. Ryback Translator,* Pergamon Press, New York.

Saedah R. Al-Mhyawi (2014). *Inhibition of mild steel corrosion using Juniperus plants as green inhibition. African Journal of Pure and Applied Chemistry*. Vol. 8(1), pp. 9-22, January, 2014. DOI:10.5897/AJPAC2013. 0497.

Sani L.M, Abdulwahab M., Yaro S. A., & Umaru O. B., (2015). *Inhibitive Effect by Psidium guajava Leaf Extract on the Corrosion of Al-Si-Mg (SSM-HPDC) Alloy in Simulated Sea water Environment*. Metall. Mater. Eng. 21(4):241-251.

Siaka A. Abdulfatai, Owa. O Sunday, M. K. Gafar, and Okunola, J O.(2021). *Corrosion inhibition efficiency, adsorption behavior, kinetics and thermodynamic studies of lannea acida ethanol leaves extract on mild steel in hydrochloric acid.* Vol. 5 No. 2, June 2021, pp 621-634 DOI: https://doi.org/10.33003/fjs-2021-0502-678

Sumra N., Shabbir H., Naureen N. M. P., Madiha R (2018). *The phytochemistry and medicinal value of Psidium guajava (guava).* Clinical Phytoscience (2018) 4:32 https://doi.org/10.1186/s40816-018-0093-8

Tan, B., He, J., Zhang, S., Xu, C., Chen, S., Liu, H., & Li, W. (2021). *Insight into the anti-corrosion nature of Betel leaves water extracts as the novel and eco-friendly inhibitors*. Journal of Colloid and Interface Science, 585 (December), 287–301. Https://doi.org/10.1016/j.jcis.2020.11.059

Thesis, A. (2009). *Investigation of the performance of some corrosion inhibitors in aerated acid solutions*.

Utility H.H, (1975). *Corrosion and Corrosion Control,*

Victoria S., Rohith Prasad, & Manivannan R. (2015). *Psidium Guajava Leaf Extract as Green Corrosion Inhibitor for Mild steel in Phosphoric Acid*. Int. J. Electrochem. Sci. 2220–2238.

Xiuli Zuo, Wenpo Li b, Wei Luo, Xin Zhang, Yujie Qiang, Jian Zhang, Hao Li, Bochuan Tan. *Research of Lilium brownii leaves extract as a commendable and green inhibitor for X70 steel corrosion in hydrochloric acid.* Journal of Molecular Liquids 321 (2021) 114914. 2020 Elsevier B.V. All rights reserved. https://doi.org/10.1016/j.molliq.2020.114914 0167-7322

Xu X, Singh A, Sun Z, Ansari KR, Lin Y. (2017). *Theoretical, thermodynamic and electrochemical analysis of biotin drug as an impending corrosion inhibitor for mild steel in 15% hydrochloric acid.* R. Soc. open sci. 4: 170933. http://dx.doi.org/10.1098/rsos.170933
y, 271 (4): 845–854.

Yanxia Liu, Wei Du, Xiuquan Yao, Chunlin Liu, Xiaofang Luo, Lei Guo, Chao Guo (2022). *Electrochemical and Theoretical Study of Corrosion Inhibition on X60 Steel in H_2SO4 Solution by Omeprazole*. Int. J. Electrochem. Sci., 17 (2022) Article Number: 220516, doi/ 10.20964/2022.04.58.